# Conference Proceedings

ECCOMAS Thematic Conference on

# MULTIBODY DYNAMICS

Prague, June 19 - 22, 2017

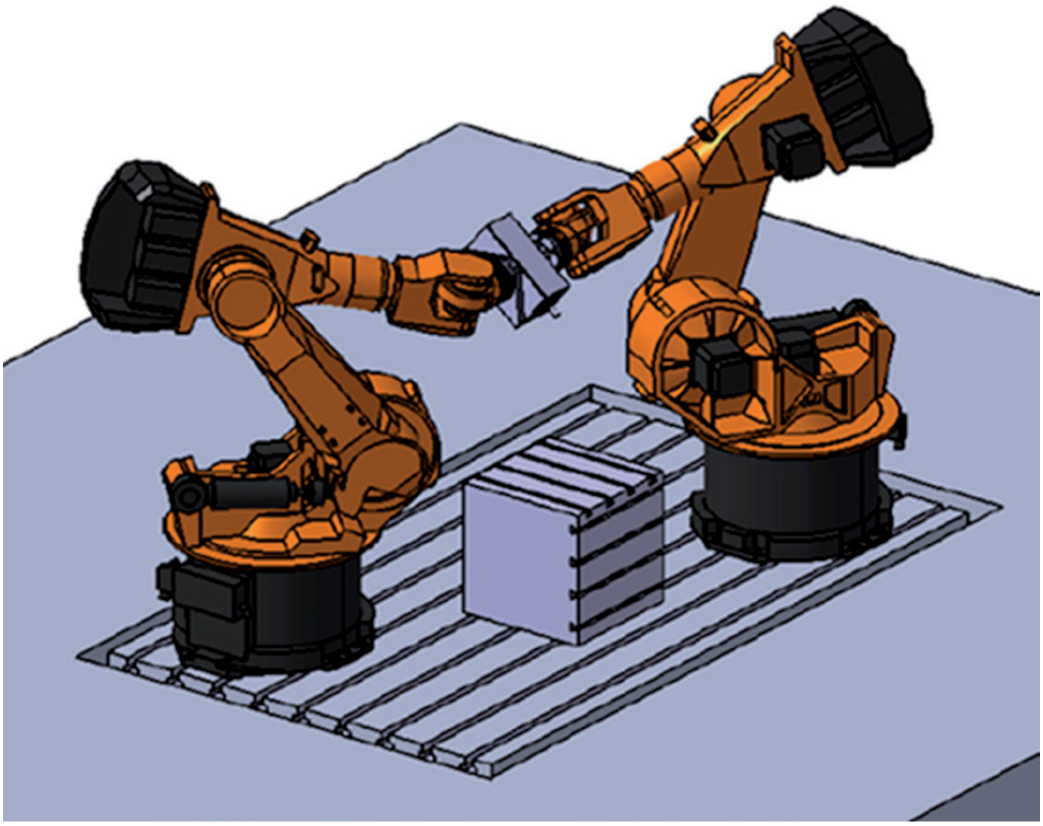

CZECH TECHNICAL UNIVERSITY IN PRAGUE
Faculty of Mechanical Engineering

CTU CZECH TECHNICAL UNIVERSITY IN PRAGUE

ECCOMAS

# Proceedings of the 8th ECCOMAS Thematic Conference on MULTIBODY DYNAMICS 2017

Prague, June 19 – 22, 2017
Faculty of Mechanical Engineering
Czech Technical University in Prague
www.multibody2017.cz

**Editors:**

Michael Valášek, Zbyněk Šika, Tomáš Vampola, Michal Hajžman, Pavel Polach, Zdeněk Neusser, Petr Beneš, Jan Zavřel

**Contact address:**

Czech Technical University in Prague
Faculty of Mechanical Engineering
Technická 4
166 07 Prague
Czech Republic
Phone: +420 22435 5038

**Design:**

Tomáš Prajs

**Publisher:**

Nakladatelství ČVUT (CTN), Zikova 1903/4, 166 36 Praha 6 – Dejvice
921 pages, 10 copies, 1. edition

ISBN 978-80-01-06173-2 (online)
ISBN 978-80-01-06174-9 (printed)

# Increase of Stiffness in Physically Cooperating Robots

Michael Valášek, Martin Nečas, Ladislav Mráz

Faculty of Mechanical Engineering
Czech Technical University in Prague
Technická 4, 166 07 Prague, Czech Republic
[Michael.Valasek, Martin.Necas]@fs.cvut.cz

## Abstract

The industrial robots have full range of spatial motion and are suitable for carrying out manufacturing operations like CNC machining. However, the industrial robots exhibit low stiffness that leads to unacceptable inaccuracies of robot motions under disturbance forces and renders industrial robots unsuitable for milling materials other then wood, plastic or similar materials. The main goal of this article is to elaborate on ways how the stiffness of industrial robots can be increased in order to enlarge their usability.

The proposed solution is to use two (or more) physically coupled robots with the inter-robotic interface carrying CNC spindle as illustrated in Fig. 1 [1], [6]. This mere mechanical coupling of robots increases the stiffness significantly but not in a sufficient manner. Other methods, such as load dependent robot deformation models have to be used as well.

**Keywords:** industrial robot, stiffness, machine tool, milling, CNC

## 1. Introduction

From the mechanical point of view there are generally only two ways how to increase the static stiffness of mechanical structures. The structures can be made more deformation resilient against the action of external force either by the use of advanced composite materials along the with sophisticated engineering design procedures or we can treat the structures as deformable and try to compensate the unwanted deformation using compensation schemes [1]. This leads to several possible scenarios with different levels of sophistication. In general four basic setups are possible: 1) one uncompensated robot 2) two or more connected uncompensated robots 3) one compensated robot and 4) two or more connected compensated robots. This article describes scenarios 2) and 3).

## 2. Stiffness Increase of Two Connected Force Uncompensated KUKA Robots

The robots setup as shown in Fig1a-b is considered. Two industrial robots are mutually connected via inter-robotic interface carrying e.g. a CNC milling spindle [1], [2].

The main obstacle in using the proposed robot configuration is the control scheme. Physical setup of two or more connected robots leads to a redundantly actuated mechanical system containing kinematic constraints. Standard control schemes have to be adjusted to cover up for this complication as there are 12 (or more) motors to control just 6 degrees of freedom of the inter-robotic interface. The actuators are mutually constrained and are not independent as it is in the case of a single robot with open kinematic loop.

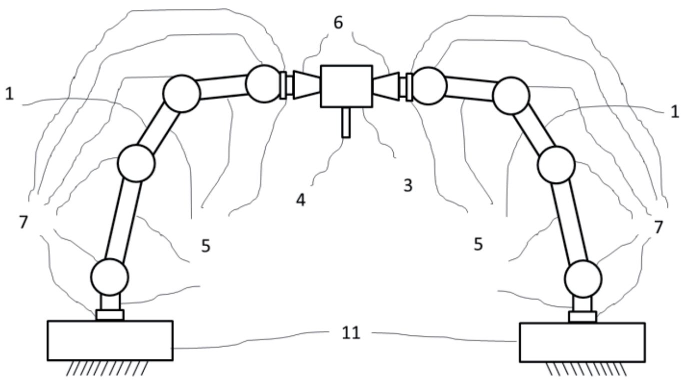


Figure 1a): The scheme of physically cooperating robots

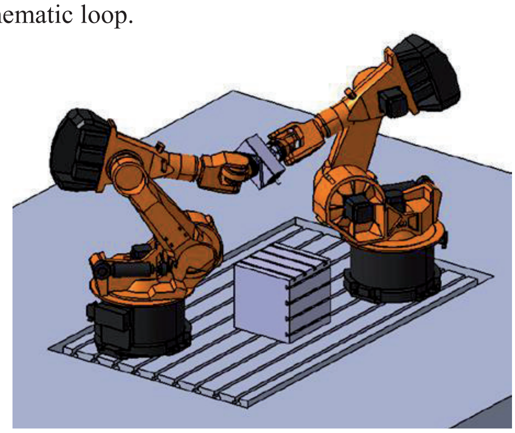

Figure 1b): The working concept

### 2.1. Dynamic model

To implement the control of a physically connected group of two KUKA robots Fig. 2, a dynamic model of one robot was first created using the composite method for dynamic equations assembly [1].

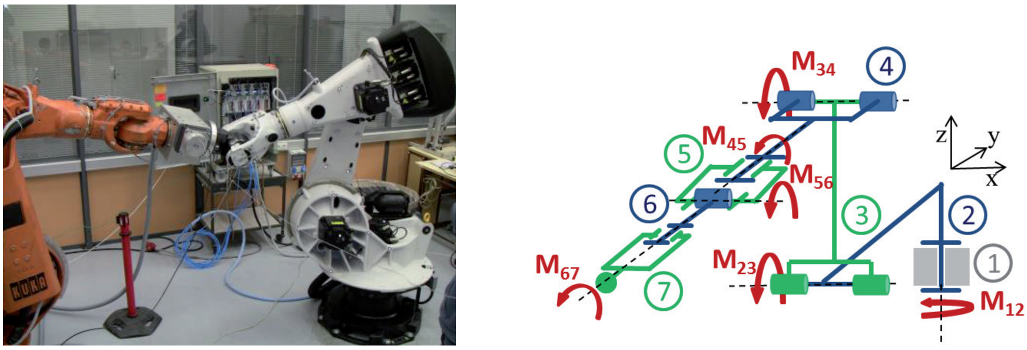


a) b)

Figure 2: Physically connected robots and kinematic model

Composite method [3] is typicaly used to construct the equations of motion for systems of flexible bodies, however here, the individual bodies are considered rigid and only shaft motors with reduced inertia of gears in individual kinematic pairs are considered to be compliant. The composite method uses relative coordinates. In order to express the overall position of the robot, a set of six relative angles is introduced:

$$\boldsymbol{q} = [\varphi_{12}, \varphi_{23}, \varphi_{34}, \varphi_{45}, \varphi_{56}, \varphi_{67},]^T$$

To express dynamic properties of individual bodies (weights, moments of inertia, deviation moments), the chosen method uses the discretization of bodies by mass points. The total weight of the robot was divided into individual bodies and discretized within individual bodies as shown in Figure 3.

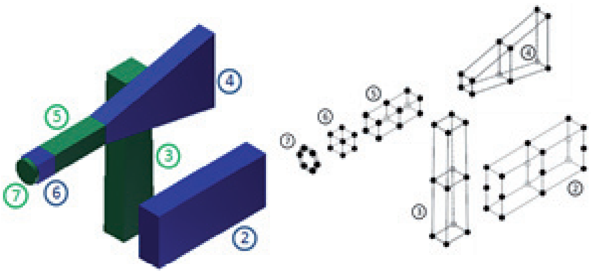


Figure 3: Simplified mass distribution in individual bodies

To assemble the equations of motion the software SymEOM based on Composite Method for Compliant Bodies [3], [4] was used. This program assembles the equations of motion by symbolic substitution of formed expressions. It eliminates superfluous expressions and classifies the formed expressions as either constants or variables to eliminate redundant arithmetic operations. The motion equations of the connected robot group were assembled in the following form [3], [5]:

$$\begin{bmatrix} \boldsymbol{M} & \boldsymbol{\phi}^T \\ \boldsymbol{\phi} & \boldsymbol{0} \end{bmatrix} \begin{bmatrix} \ddot{\boldsymbol{s}} \\ -\boldsymbol{\lambda} \end{bmatrix} = \begin{bmatrix} \boldsymbol{Q}(\boldsymbol{F_{EP}}, \boldsymbol{n}, \boldsymbol{s}, \dot{\boldsymbol{s}}) \\ \boldsymbol{P}(\boldsymbol{s}, \dot{\boldsymbol{s}}) \end{bmatrix} \tag{1}$$

In the equation of motion (1) the vector $\boldsymbol{s}$ includes the vectors of relative arm angles $\boldsymbol{q_1}$ and $\boldsymbol{q_2}$ of the first and the second robot and the vectors of rotation angles $\boldsymbol{q_{M1}}$ a $\boldsymbol{q_{M2}}$ of the first and second robot: $\boldsymbol{s} = [\boldsymbol{q}, \boldsymbol{q_M}]$; $\boldsymbol{q} = [\boldsymbol{q_1}, \boldsymbol{q_2}]$; $\boldsymbol{q_M} = [\boldsymbol{q_{M1}}, \boldsymbol{q_{M2}}]$.The $\boldsymbol{\lambda}$ vector is a vector of Lagrange multipliers. The flexibility in the robot gearboxes leads to a system that acquires a double number of degrees of freedom as illustrated by the composite state vector $\boldsymbol{s}$ of the entire dynamic system of the connected robots containing the vectors $\boldsymbol{q}$ a $\boldsymbol{q_M}$.

Matrix $\boldsymbol{M}$ is a mass matrix corresponding to the established relative coordinates. The matrix $\boldsymbol{\phi}$ is Jacobi matrix expressing constraints due to the kinematic loop. The vector $\boldsymbol{Q}(\boldsymbol{n}, \boldsymbol{s}, \dot{\boldsymbol{s}})$ is a vector of generalized forces that depends on $\boldsymbol{s}$ and $\dot{\boldsymbol{s}}$ and on servodrives torque vector $\boldsymbol{n} = [\boldsymbol{n_1}, \boldsymbol{n_2}]$**.** Torques $\boldsymbol{n_1}$ and $\boldsymbol{n_2}$ correspond to the first and second robot respectively. In addition, the vector $\boldsymbol{Q}$ depends on the force vector acting on the spindle end-effector: Force $\boldsymbol{F_{EP}}$ is consider to have three components corresponding to the Cartesian force components. This force simulates the technological forces due to the machining process.

Vector $\boldsymbol{P}(\boldsymbol{s}, \dot{\boldsymbol{s}})$ contains acceleration residues that originates from the rigid connection between the robots. To avoid constraints violation Baumgart stabilization [5] is contained in the term $\boldsymbol{P}(\boldsymbol{s}, \dot{\boldsymbol{s}})$**.**

### 2.1.1. The Control Scheme

The system can be classified as a MIMO system with six outputs (6 degrees of freedom of rotation and position of the connection platform) and 12 inputs (2 x 6 = 12 motors). This means that the number of motors is twice redundant. Due to this internal constraint a simple application of cascade control is not possible. It is necessary to introduce an approach that will suppress the push-pull behavior of the drives and the mutual power antagonism when using classical PID cascade control scheme.

### 2.1.2. Torque Compensation in Cascade Control Scheme

The mutual motors hunting was resolved by the process of torque compensation at the drives. This procedure is as follows: The regulators provide the desired torques $\boldsymbol{n_d}$ of the individual motors. Such moments result in the required force $\boldsymbol{F_d}$ acting on the end-effector whose trajectory is monitored and controlled. Dependent coordinates (due to the connection) of the robots are designated as $\boldsymbol{z}$, the independent endpoint coordinates are denoted as $\boldsymbol{x_{EP}}$. Between these coordinates, respectively velocities exists the following transformation:

$$\dot{\boldsymbol{z}} = \frac{\partial \boldsymbol{\varphi}}{\partial \boldsymbol{x_{EP}}} \dot{\boldsymbol{x}}_{\boldsymbol{EP}} = \boldsymbol{J} \cdot \dot{\boldsymbol{x}}_{\boldsymbol{EP}} \tag{2}$$

Based on kinetostatics, the transformation between forces $\boldsymbol{F_d}$ and moments $\boldsymbol{n_d}$ can be established as:

$$\boldsymbol{F_d} = \boldsymbol{J^T n_d} \tag{3}$$

The equation (3) represents an under constrained system and the solution of this system that minimizes the values of required moments $\boldsymbol{n_d}$ can be obtained by right Moore-Penrose pseudoinverse

$$\boldsymbol{n_d} = \boldsymbol{J}(\boldsymbol{J^T J})^{-1} \boldsymbol{F_d} \tag{4}$$

In this way, the control torques are compensated at the torque control level and the mutual hunting of the drives is eliminated. The control diagram is therefore expanded by the compensation block, see Fig. 4. The diagram contains blocks representing dynamic robot models, nested blocks of cascade control, and a block representing moment compensation to suppress the mutual antagonistic motor hunting effect.

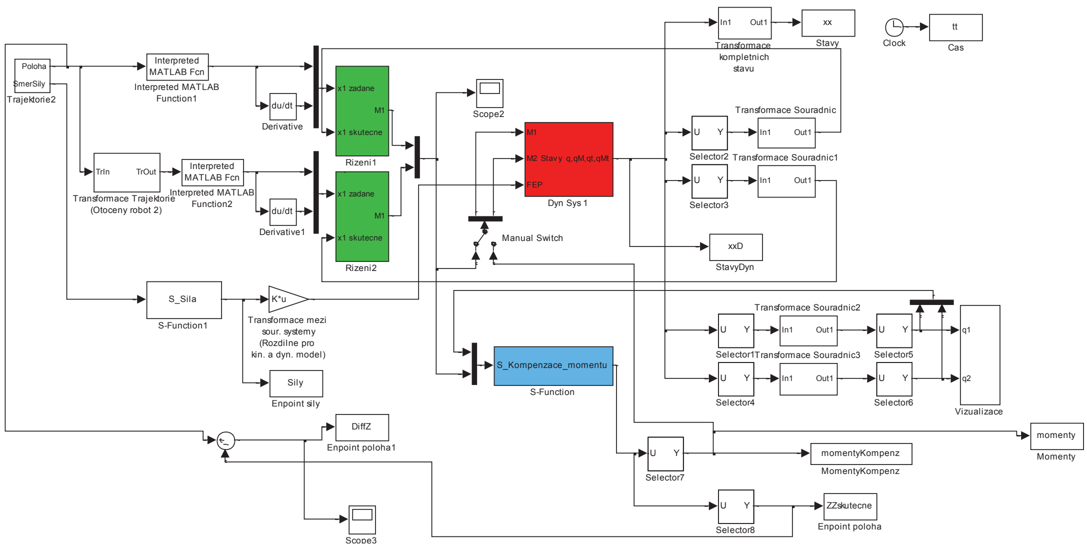


Figure 4: Simulation scheme of the connected group of robots with compensation block

### 2.1.3. Basic Simulation Results

Figure 5 shows the simulation results for the motion along the circular path along with the 3D visualization environment used to visualize the group of two connected KUKA robots.

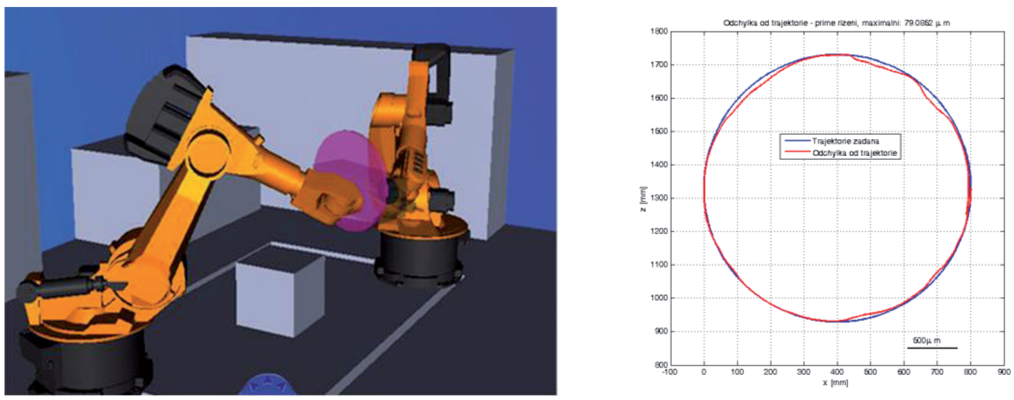

Figure 5: 3D simulation environment with simulation of a circular motion.

## 3. Stiffness Increase of One KUKA Robot – Disturbance Force Compensation Scheme

The force exerted on the end-point of the robot during CNC milling causes robot structure deformation. This results in a deviation from the desired trajectory. Therefore, it is necessary to create an algorithm to compensate these deformations. The overall deformation of the robot is formed by torsional deformation in the individual gearboxes (the dominant part) and then the bending deformation of the individual arms (the minor part). The individual robot axes are equipped with an additional angular measurement systems that identify the relative rotation of adjacent parts of the robot. In this way, the deformation of the gearboxes can be determined. Bending arm deformation cannot be directly measured. Consequently, arm compliances must be identified experimentally. Based on the known robot load, the dominant bending deformations can be estimated.

The load on the robot is not known in general unless end-effector force sensor is used. However, this force can be determined from the additional measurement system mounted directly between respective robot axes. CNC milling process generally does not introduce major loading moments at the end-effector, therefore only the disturbance force loading is considered.

In order to compensate the load induced deformations, an experimental identification of the gearboxes torsional stiffness and the flexural flexibilities of the arms was done. Afterwards, a force estimation model acting on the robot end-effector was developed. And ultimately, the resulting kinematic deformation model based on partial Robot end-effector force prediction model was assembled.

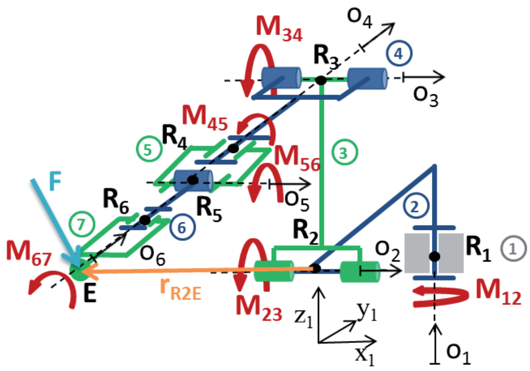


Figure 6: Kinematic diagram of a robot loaded with a force at the end-efector

The force acting on the end-effector of the robot (Fig. 6) exerts torques on the individual gearboxes and thus causes their torsional deformations. Using additional measurement we can determine the precise rotation between respective robot links. Besides, we also know the exact angular position of the motor between these links. The difference in these rotations gives a torsional deformation that is proportional to the torque that causes this deformation. The constant of proportionality is, of course, the rigidity of the motor drive unit (motor + gearbox) that has been determined experimentally. We are able to obtain information about the deformations and therefore the loading torques for all six axes of the robot. From this information, the force acting on the end-effector can already be determined by the following procedure:

If we load the robot end-effector with the force $\boldsymbol{F}$ (Fig. 6), it will exert at the individual robot locations $R_1, R_2, \ldots, R_6$ corresponding torques:

$$\boldsymbol{M}_{Ri} = \boldsymbol{r}_{RiE} \times \boldsymbol{F} = \tilde{\boldsymbol{r}}_{RiE} \boldsymbol{F} \quad (5)$$

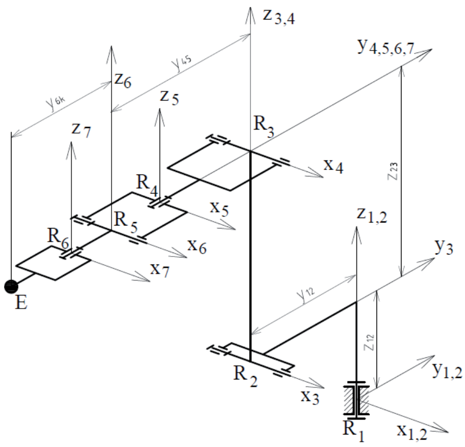


Figure 7: Coordinate systems on individual bodies

Here $\boldsymbol{r}_{RiE}$ marks the vector between the points $\boldsymbol{R_i}$ and the point of force application $\boldsymbol{E}$ (in Fig. 6) is indicated by vector $\boldsymbol{r_{R2E}}$. All vectors are expressed in fixed coordinate system $x_1y_1z_1$. The symbol $\tilde{\boldsymbol{r}}_{\boldsymbol{RiE}}$ represents an antisymmetric matrix obtained from the vector $\boldsymbol{r_{RiE}}$.

To describe the position of individual points $\boldsymbol{R_i}$ and $\boldsymbol{E}$ in the coordinate system 1 transformation matrixes describing the relative positions of coordinate systems must be assembled. (Fig. 7). These transformations have the following structure[1]:

$$\begin{gathered}\boldsymbol{T}_{12}=\boldsymbol{T}_{\varphi z}(\varphi_{12})\boldsymbol{T}_z(z_{12})\boldsymbol{T}_y(y_{12})\\ \boldsymbol{T}_{23}=\boldsymbol{T}_{\varphi x}(\varphi_{23})\boldsymbol{T}_z(z_{23})\\ \boldsymbol{T}_{34}=\boldsymbol{T}_{\varphi x}(\varphi_{34})\boldsymbol{T}_y(y_{45})\\ \boldsymbol{T}_{45}=\boldsymbol{T}_{\varphi y}(\varphi_{45})\\ \boldsymbol{T}_{56}=\boldsymbol{T}_{\varphi x}(\varphi_{56})\\ \boldsymbol{T}_{67}=\boldsymbol{T}_{\varphi y}(\varphi_{67})\end{gathered} \tag{6}$$

The expanded position vectors of individual points are then obtained as:

$$\begin{gathered}\boldsymbol{r}_{R1}=[0\quad 0\quad 0\quad 1]^{\boldsymbol{T}}\\ \boldsymbol{r}_{R2}=\boldsymbol{T}_{12}\cdot[0\quad 0\quad 0\quad 1]^{\boldsymbol{T}}\\ \boldsymbol{r}_{R3}=\boldsymbol{T}_{12}\boldsymbol{T}_{23}\cdot[0\quad 0\quad 0\quad 1]^{\boldsymbol{T}}\\ \boldsymbol{r}_{R4}=\boldsymbol{T}_{12}\boldsymbol{T}_{23}\boldsymbol{T}_{34}\cdot[0\quad 0\quad 0\quad 1]^{\boldsymbol{T}}\\ \boldsymbol{r}_{R5}=\boldsymbol{T}_{12}\boldsymbol{T}_{23}\boldsymbol{T}_{34}\boldsymbol{T}_{45}\cdot[0\quad 0\quad 0\quad 1]^{\boldsymbol{T}}\\ \boldsymbol{r}_{R6}=\boldsymbol{T}_{12}\boldsymbol{T}_{23}\boldsymbol{T}_{34}\boldsymbol{T}_{45}\boldsymbol{T}_{56}\cdot[0\quad 0\quad 0\quad 1]^{\boldsymbol{T}}\\ \boldsymbol{r}_{R6}=\boldsymbol{T}_{12}\boldsymbol{T}_{23}\boldsymbol{T}_{\boldsymbol{34}}\boldsymbol{T}_{45}\boldsymbol{T}_{56}\cdot\boldsymbol{T}_{67}[0\quad 0\quad 0\quad 1]^{\boldsymbol{T}}\\ \boldsymbol{r}_{E}=\boldsymbol{T}_{12}\boldsymbol{T}_{23}\boldsymbol{T}_{\boldsymbol{34}}\boldsymbol{T}_{45}\boldsymbol{T}_{56}\cdot\boldsymbol{T}_{67}[0\quad y_{6k}\quad 0\quad 1]^{\boldsymbol{T}}\end{gathered} \tag{7}$$

The individual vectors $\boldsymbol{r}_{RiE}$ are:

$$\boldsymbol{r}_{RiE}=\boldsymbol{r}_E-\boldsymbol{r}_{Ri} \tag{8}$$

The moments that produce torsional deformations at respective drive units are obtained by the corresponding projections of moments $\boldsymbol{M_{Ri}}$ on the directions of the robot axes:

$$M_{oi}=\boldsymbol{o}_{\boldsymbol{i}}^{T}\boldsymbol{M}_{\boldsymbol{Ri}} \tag{9}$$

Here $\boldsymbol{o_i}$, denotes the unit vector defining the robot axis (1 to 6). The unit vectors of the local axes represent the columns of the directional cosine matrices of the individual transformations. Direction cosine matrix $\boldsymbol{S}_{0i}$ is obtained by removal of the last row and column in the homogeneous transformation matrix $\boldsymbol{T}_{0i}$.

Torsional deformations of the drive units $\delta_i$ can be directly determined from the installed measurement systems. This deformation must correspond to the torque applied to the drive unit:

$$K_i\delta_i=M_{oi} \tag{10}$$

In (10) coefficients $K_i$ stand for torsional rigidity of the drive units (gearbox + motor). By substituting (5) and (9) into (10) we obtain:

$$K_i\delta_i=\boldsymbol{o}_{\boldsymbol{i}}^{T}\tilde{\boldsymbol{r}}_{\boldsymbol{RiE}}\boldsymbol{F} \tag{11}$$

These equations can be assembled for all six joints of the robot and constitute a redundant over constrained system of equations to determine the three components of the force $\boldsymbol{F}$:

$$\begin{bmatrix}\boldsymbol{o}_{\boldsymbol{1}}^{T}\tilde{\boldsymbol{r}}_{\boldsymbol{R1E}}\\ \boldsymbol{o}_{\boldsymbol{2}}^{T}\tilde{\boldsymbol{r}}_{\boldsymbol{R2E}}\\ \vdots\\ \boldsymbol{o}_{\boldsymbol{6}}^{T}\tilde{\boldsymbol{r}}_{\boldsymbol{R6E}}\end{bmatrix}\boldsymbol{F}=\begin{bmatrix}K_1\delta_1\\ K_2\delta_2\\ \vdots\\ K_6\delta_6\end{bmatrix} \tag{12}$$

It is then possible to write the equation (12) as:

[1] Here, for the sake of simplicity, the transformations are given for the nominal robot kinematic model without calibration parameters in the enhanced kinematicly calibrated model.

$$\boldsymbol{A} \cdot \boldsymbol{F} = \boldsymbol{M_o} \tag{13}$$

Equation (13) can then be solved for the unknown force $\boldsymbol{F}$ by using a Moore–Penrose pseudoinverse:

$$\boldsymbol{F} = (\boldsymbol{A}^{\boldsymbol{T}}\boldsymbol{A})^{-\boldsymbol{1}}\boldsymbol{A}^{\boldsymbol{T}}\boldsymbol{M_o} \tag{14}$$

In this way, the force acting on the robot end-effector is determined.

### 3.1. Determination of Robot Arm Deformation

The force acting on the robot's end-effector causes torsional deformation in gearboxes, this deformation can be measured directly. This force, however, also causes the bending deformation of the robot arms. To determine the bending deformation of the individual arms of the robot, it is possible to look at them as beams loaded at the end with force and torque (Fig. 8). These force effects are, of course, produced by a force acting on the robot end-effector. This force is estimated by the equation (14). The same force acts also at the ends of the individual robot links (at points $\boldsymbol{R_2}$ till $\boldsymbol{R_6}$ and $\boldsymbol{E}$), but in addition, it adds the bending moment due to the force $\boldsymbol{F}$. This moment is expressed in equation (5). In order to express the beam bending effects due to the force $\boldsymbol{F}$ these deformation effects have to be expressed in local axes of the individual robot links. The forces and moments expressed in the individual local axes of the given robot links are:

$$\begin{bmatrix} F_{xi} \\ F_{yi} \\ F_{zi} \end{bmatrix} = \boldsymbol{S}_{0i}^T \cdot \boldsymbol{F}, \qquad \begin{bmatrix} M_{xi} \\ M_{yi} \\ M_{zi} \end{bmatrix} = \boldsymbol{S}_{0i}^T \cdot \boldsymbol{M}_{Ri} \tag{15}$$

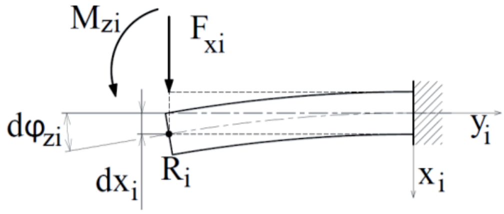


Figure 8 The robot arm modeled as cantilevered beam

Figure 8 illustrates a beam having a longitudinal axis *y*, which is deformed in the *xy* plane. Beam sag $dx_i$ at the end of the beam and rotation $d\varphi_{zi}$ can be calculated as:

$$\begin{bmatrix} dx_i \\ \varphi_{zi} \end{bmatrix} = \begin{bmatrix} \alpha_i & \gamma_i \\ \beta_i & \delta_i \end{bmatrix} \begin{bmatrix} Fx_i \\ M_{zi} \end{bmatrix} \tag{16}$$

Constants $\alpha_i, \beta_i, \gamma_i, \delta_i$ represent influence coefficients that are to be determined experimentally. In the same way as in equation the (16) it is possible to determine the deformation $dz_i$ a $d\varphi_{xi}$ in plane $yz$. If the beam has longitudinal axis $z$, the lateral deformations $dx_i, dy_i, d\varphi_{yi}, d\varphi_{xi}$ are determined similarly. None of the robot links has a longitudinal axis $x$.

### 3.2. The Resulting Position of the End-Effector

The position of the robot end-effector is dominantly affected by the deformation in the gearboxes and by bending deformations of the individual robot links. In the previous chapters it was shown how these deformations can be evaluated. In order to determine the exact position of the robot's end-effector, the resulting kinematic transformation must be adjusted to accommodate for these additionally evaluated deformations. The position of the robot end-effector is then expressed as:

$$\begin{gathered} \boldsymbol{r}_E = \boldsymbol{T}_{12}^d \boldsymbol{T}_x(dx_2) \boldsymbol{T}_z(dz_2) \boldsymbol{T}_{\varphi x}(d\varphi_{x2}) \boldsymbol{T}_{\varphi z}(d\varphi_{z2}) \\ \boldsymbol{T}_{23}^d\, \boldsymbol{T}_x(dx_3) \boldsymbol{T}_y(dy_3) \boldsymbol{T}_{\varphi x}(d\varphi_{x3}) \boldsymbol{T}_{\varphi y}\big(d\varphi_{y3}\big) \\ \boldsymbol{T}_{34}^d \boldsymbol{T}_{45}^d \boldsymbol{T}_x(dx_5) \boldsymbol{T}_z(dz_5) \boldsymbol{T}_{\varphi x}(d\varphi_{x5}) \boldsymbol{T}_{\varphi z}(d\varphi_{z5}) \\ \boldsymbol{T}_{56}^d \boldsymbol{T}_{67}^d [0 \quad y_{6k} \quad 0 \quad 1]^T \end{gathered} \tag{17}$$

The matrix $\boldsymbol{T}_{i,i+1}^d$ expresses the homogenous transformation between systems $i$ and $i+1$, taking into account also the torsional deformation of the drive units. The resulting transformation therefore correspond to the equations (6), with the difference that the individual deflections at the gearboxes $\delta_i$ are also concidered:

$$\varphi_{i,i+1} = \varphi_{i,i+1} + \delta_i \tag{18}$$

In this way, the relation for the determination of the position of the end-effector of the robot model is enhanced and the robots performance in low speed operations can be improved.

The robot gearbox stiffness coefficients along with compliance characteristics of individual robot bodies were evaluated experimentally. Robot was loaded in 4 defined configurations (Fig. 9) and the deformation was monitored using dial gauges and the laser tracker Leica AT901 MR at specific points $R_2, R_3$ a $R_5$ on the robot axes and the end-point $E$ (Fig. 2 b). From the measurements in these 4 configurations the necessary influence coefficients were determined.

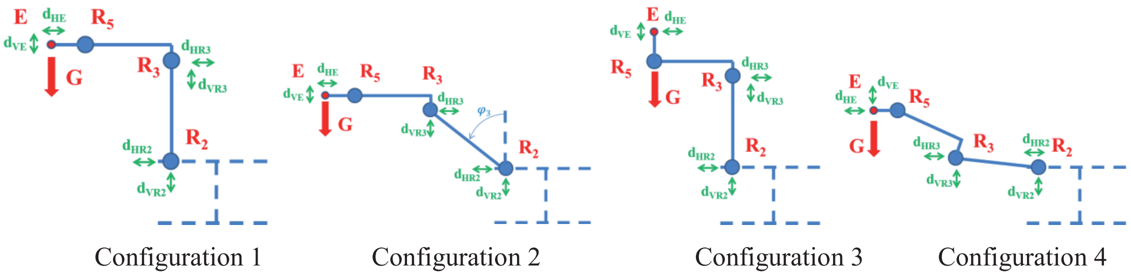


Figure 9: Configuration for determination of robot stiffness parameters

### 3.3. Experimental Evaluation of the Prediction Model

The deformation estimation model was tested for the configurations 1 through 4 (Fig. 4). The deformation of the robot end-effector was measured horizontally and vertically using dial gauges and computed by the model. The results are shown in Fig. 10-17, where dashed lines correspond to the predicted deformations and solid lines to the deformations actually measured.

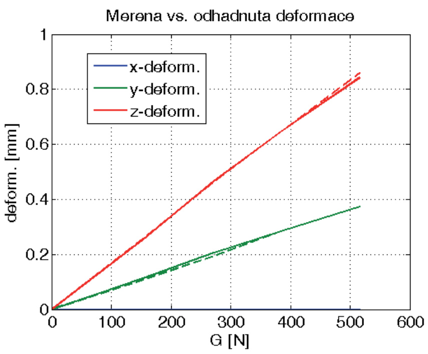


Figure 10: End-point deformation, configuration 1

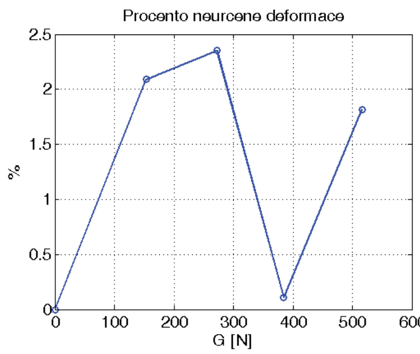


Figure 11: Percentage of undetermined deformation, configuration 1

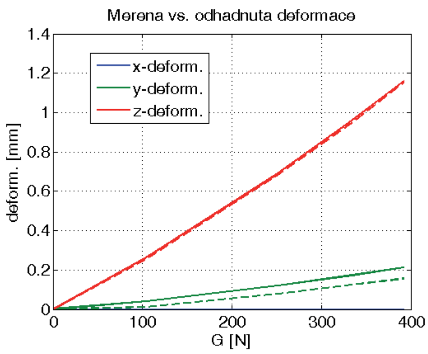


Figure 12: End-point deformation, configuration 2

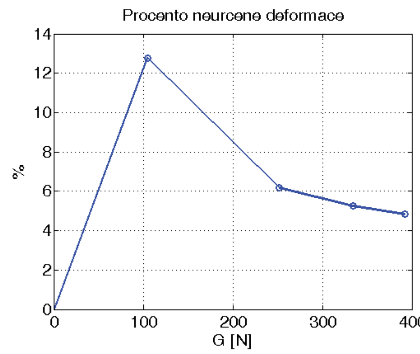


Figure 13: Percentage of undetermined deformation, configuration 2

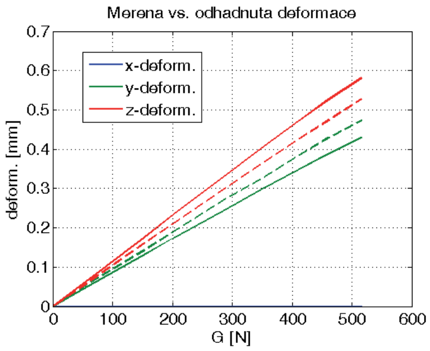


Figure 14: End-point deformation, configuration 3

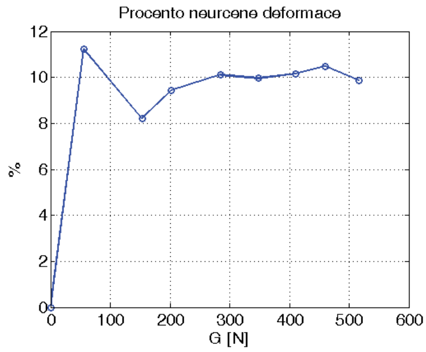


Figure 15: Percentage of undetermined deformation, configuration 3

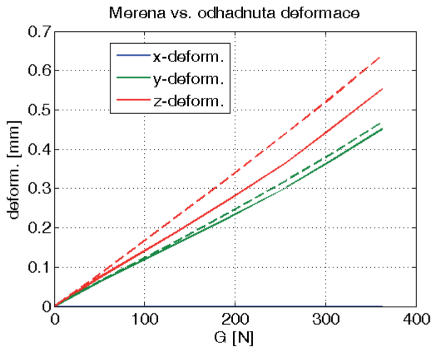


Figure 16: End-point deformation, configuration 4

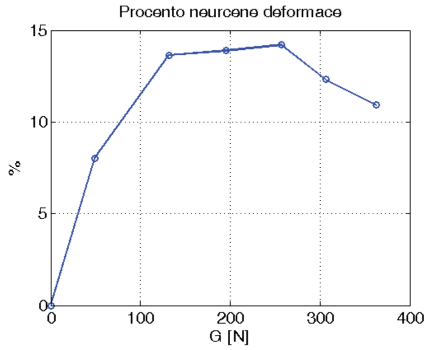


Figure 17: Percentage of undetermined deformation, configuration 4

As can be seen from the test results, it is possible to determine the deformation of the robot end-effector with the satisfactory precision [6]. The maximum undetermined deformation is approximately 15% for the configuration 4 (Fig 9). This is a positive result from the viewpoint of increasing robot stiffness: The robot stiffness at the end-effector is given by the ratio:

$$K_E = \frac{F}{d} \tag{19}$$

Where the force $F$ is the force acting on the end-effector, and the deformation $d$ is the total deformation. If the proportion $u$ of the total deformation $d$, $d_{determined} = u \cdot d$ can be determined, then it is also possible to fully compensate it. Deformation that remains uncompensated can be expressed as $d_{undetermined} = (1-u) \cdot d$. This leads to the new robot's rigidity:

$$K_{Enew} = \frac{F}{(1-u)d} = \frac{1}{(1-u)} K_E \tag{20}$$

Lower the percentage of deformation that the model fails to identify, the higher the robot stiffness. Undetermined deformation of 15% $(u = 85\%)$ leads to approximately sevenfold increase of robot stiffness.

The total robot stiffness $K_E$ determined at the robot end-effector is about 0,6 $N/\mu m$.. The seven-fold increase gives the stiffness of 4,2 $N/\mu m$.. When measured on combined robots, their stiffness was estimated to increase approximately by factor of 3.5. In this way, it is possible to increase the stiffness to approximately 14 $N/\mu m$, thereby making the suggested coupled robots configuration as viable alternative to conventional CNC machines.

## 4. Conclusions

This paper presented several concepts how the mechanical stiffness of industrial robots could be increased. The first approach suggested the use of more of mutually connected robots to take the advantage of closed kinematic loops providing stiffness increase due to frame-like structure. The second approach, currently developed for single robot, is based on the use of additional sensors measuring the axial deformation between servomotor encoder and actual robot revolute axes to estimate and compensate robot deformations using deformation model.

The stiffness values of each robot gearbox and the parameters describing the compliance of its robot links were experimentally identified. A model that predicts the force acting on the robot end-effector based on information from the additional displacement of its individual axes has been developed in a detail. Based on this force, the deformation of the individual robot components is then predicted and the total deformation at its end-effector is determined from these partial deformations. The results of the experiments carried out in different configurations have shown that approximately 85% of the overall deformation can be estimated, (often even more). Such a prediction of deformation results in approximately a seven-fold increase in the overall stiffness of one robot. The combination of two robots also shows a stiffness increase of about 3.5 times. The resulting stiffness allows the robots to be possibly used for CNC machining with the accuracy getting closer to the conventional CNC machines. Further work will be devoted to combination of these two approaches.

## Acknowledgments

This work was supported by the Project Rob4Ind4.0 CZ.02.1.01/0.0/0.0/15_003/0000470 and the European Regional Development Fund. This support is gratefully acknowledged.

## References

[1] M. Valasek, M. Necas and L. Binar, Method of determining a position of a cutting tool center fastened in a cooperating clamping head and cooperating clamping head and the cooperating clamping head, Patent CZ2012474/EP2743040A2, UPV, Prague, 2012.

[2] M. Valasek, V. Bauma, Z. Sika and O. Svatos, A method and a device for change of rigidity of a serial or parallel basic movable mechanism, especially of industrial robots and machine tools, CZ304673/EP2705934A2, UPV, Prague, 2014.

[3] T. Vampola, "Effective algorithm for assembly of equations of motion for compliant multi-body systems (in Czech)," Faculty of Mechanical Engineering, Czech Technical University in Prague, 1996.

[4] L. Mraz, "Symbolic generation of equation of motion for compliant multi-body systems (in Czech)," Master Thesis, Faculty of Mechanical Engineering, Czech Technical University in Prague, 2009.

[5] V. Stejskal and M. Valasek, Kinematics and Dynamics of Machinery, Marcel Dekker, New York, 1996.

[6] M. Valasek, M. Necas and L. Binar, Robotic milling center, UV 24627, UPV, Prague 2012.